The effects of carbon incorporation on the refractive index of PECVD silicon oxide layers

Cite as: AIP Advances **10**, 045331 (2020); https://doi.org/10.1063/1.5142017
Submitted: 09 December 2019 . Accepted: 07 April 2020 . Published Online: 23 April 2020

Benjamin Torda, Lazhar Rachdi, Asmaa Mohamed Okasha Mohamed Okasha, Pierre Saint-Cast, and Marc Hofmann

COLLECTIONS

Paper published as part of the special topic on Chemical Physics, Energy, Fluids and Plasmas, Materials Science and Mathematical Physics

ARTICLES YOU MAY BE INTERESTED IN

On the redistribution of charge in $La_{0.7}Sr_{0.3}CrO_3/La_{0.7}Sr_{0.3}MnO_3$ multilayer thin films
AIP Advances **10**, 045113 (2020); https://doi.org/10.1063/1.5140352

Steady state densities in a plasma confined by a dipole magnet: Diffusion induced transport explored through direct measurements and modeling
AIP Advances **10**, 045328 (2020); https://doi.org/10.1063/5.0003736

Precision current measurement with thermal-drift-minimized offset current for single-parameter electron pumps based on gate-switching technique
AIP Advances **10**, 045332 (2020); https://doi.org/10.1063/5.0002587

© 2020 Author(s).

The effects of carbon incorporation on the refractive index of PECVD silicon oxide layers

Cite as: AIP Advances 10, 045331 (2020); doi: 10.1063/1.5142017
Submitted: 9 December 2019 • Accepted: 7 April 2020 •
Published Online: 23 April 2020

Benjamin Torda, Lazhar Rachdi, Asmaa Mohamed Okasha Mohamed Okasha, Pierre Saint-Cast, and Marc Hofmann[a)]

AFFILIATIONS

Fraunhofer Institute for Solar Energy Systems ISE, Heidenhofstraße 2, 79110 Freiburg, Germany

[a)]Author to whom correspondence should be addressed: marc.hofmann@ise.fraunhofer.de

ABSTRACT

Silicon oxide (SiO_x) has many applications, including as a low-refractive index material. Plasma enhanced chemical vapor deposition (PECVD) processes are facile, low temperature routes to produce thin SiO_x layers. A route to decrease the refractive index of SiO_x films is to increase the layer porosity although maintaining structural and optical stability remains challenging. Organic carbon-containing sacrificial layers have been shown to modify the growth and resulting structure of PECVD SiO_x layers. In this work, we study the effect of adding methane (CH_4) to the standard SiO_x process gas mixture (silane and nitrous oxide) and varying deposition temperatures and microwave power in an industrial-scale, microwave PECVD reactor. Spectral ellipsometry was used to measure the optical properties of deposited layers, Fourier-transformed infrared (FTIR) spectroscopy to determine bonding and the layer porosity, and optical emission spectroscopy to characterize the plasma. We propose two regimes characterized by whether adding CH_4 increases or decreases the refractive index and porosity of deposited layers compared to SiO_x layers grown under standard conditions. However, the magnitude of the effect of adding CH_4 was not large and would not find industrial application. Furthermore, the deposited layers' refractive indices increased over time, indicating that the effects of adding CH_4 to the process gas mixture were not stable. To help explain our results and to provide guidance for future efforts to better control the refractive index of PECVD SiO_x layers via carbon incorporation while maintaining layer stability, we propose possible growth pathways for our layers considering both plasma reactions and surface processes.

© 2020 Author(s). All article content, except where otherwise noted, is licensed under a Creative Commons Attribution (CC BY) license (http://creativecommons.org/licenses/by/4.0/). https://doi.org/10.1063/1.5142017

I. INTRODUCTION

Materials with low refractive indices have a variety of applications, ranging from antireflection coatings to optical guides and light emitting diodes (LEDs).[1] Fundamentally, the refractive index (n) determines the amount of light that is reflected at an interface between two layers, as described by the well-known Snell's law. Therefore, controlling a layer's refractive index is vital to design materials with optimized optical properties.

Currently, few high density, low refractive index materials (with n values less than 1.4) exist that are also easy to produce.[1] The refractive indices, for example, of silica (SiO_2) and magnesium fluoride (MgF_2) are 1.46 and 1.39 (also reported as 1.38), respectively.[1,2] Layer density is important for structural integrity. Finding new materials, or modified existing materials, with lower n values would improve the performance of devices across a wide range of applications.

Silica, besides its relatively low n value, has many industrial uses due to its physical, optical, and electrical properties.[3] One method to modify the refractive index of SiO_2 is to increase the layer porosity.[2,4] With an increase in the porosity, the percentage of voids in the material also increases. Since air has a refractive index of roughly 1.0, this lowers the effective refractive index of SiO_2. Modifying the porosity of these layers has led to n values between 1.10 and 1.46.[2] For industrial applications, however, the production process of any material is also critical.

© Author(s) 2020

A variety of manufacturing methods exist for porous SiO_2. These include wet chemical processes, such as sol–gel deposition, liquid-phase deposition, and electrochemical oxidation of glass substrates; thermal evaporation; and plasma enhanced chemical vapor deposition (PECVD).[4,5] PECVD has the advantages of producing more homogeneous layers, allowing for easier layer deposition at relatively low temperatures, and the potential for higher throughput without wet chemicals.[4]

In 2001, Nagel *et al.* reported using a remote microwave PECVD reactor and the standard production gases silane (SH_4) and nitrous oxide (N_2O) to deposit porous SiO_2 films.[4] At high pressure and increasing distance between their plasma source and the glass substrate, they obtained refractive indices as low as 1.11. Lower n values, in turn, led to a decrease in reflection in the 400–1150 nm wavelength range most important for solar cell applications. However, the authors note that the scratch resistance of the layers (i.e., structural stability) was poor, limiting the application of the layers.

More recently, Kakiuchi *et al.* reported using a very high-frequency (150 MHz) power source with a cylindrical rotary electrode in an atmospheric pressure CVD system to deposit SiO_x layers with n values (at 632.8 nm) as low as 1.24 from mixtures of helium, SiH_4, and carbon dioxide at very high deposition rates.[6] The lower refractive indices they reported arose from increased porosity in the layers. However, the n values of samples, when less than 1.4, rose over time. The authors reported that this structural instability could also limit the scratch resistance of the layers. Finally, they suggested that increasing hydrogen (H) concentration in the plasma could help prevent condensation reactions of the film-forming radicals in the plasma. This in turn could produce films with finer structures, increasing the stability.

In 2004, Barranco *et al.* reported using a sacrificial organic layer to control the morphology of SiO_x films deposited using PECVD.[7] They were thus able to increase the porosity of the SiO_x layers and to decrease the reflectance of the films grown on glass substrates. The authors proposed that the organic layer's short carbonaceous chains were highly oxidized and subsequently removed along with simultaneous SiO_2 deposition. In their proposed growth model, the presence of the organic layer modified the nucleation and growth steps of the SiO_2 films, thereby controlling the porosity of the layers. SiO_x deposition processes utilizing carbon-based surface complexes could therefore provide promising routes to control the layer porosity.

In this work, we report our experiments adding methane (CH_4) to the standard SiO_x process gas mixture (of SiH_4 and N_2O) in an industrial scale, microwave PECVD reactor. The goal was to decrease the refractive index by controlling the layer growth and the resulting porosity. We report the effect of increasing the percentage of CH_4, while maintaining the same ratio of N_2O to SiH_4, on the refractive index as measured by ellipsometry. In addition to the process gas mixture, we varied the deposition temperature and maximum power of our reactor, observing the effect on n. Fourier-transformed infrared (FTIR) spectroscopy gave insight into the bonding and structure of the deposited layers, while we characterized the plasma for different processing conditions using optical emission spectroscopy (OES). Finally, we propose a possible growth pathway for porous SiO_x under our deposition conditions.

II. EXPERIMENTAL

A. Experimental procedure

Figure 1 presents a graphical view of the experimental procedure.

B. Sample preparation

Thin films were deposited on planar (shiny etched), p-type (boron-doped) float zone (FZ) silicon wafers (Siltronic, 250 nm, 0.8–1.2 Ω cm). Before deposition, the FZ wafers were manually cut to roughly 2 × 2 cm^2 samples and labeled. Next, the samples were dipped in hydrofluoric acid (HF, 1%) for 1 min to hydrogenate the silicon surface and remove any surface oxidation. After the HF dip, the samples were quickly dipped in deionized water and then immediately dried using nitrogen (N_2) gas.

C. Deposition

Thin films were deposited in an industrial microwave MAiA PECVD reactor (Meyer Burger AG) from mixtures of gaseous SiH_4, N_2O, and CH_4. Figure 2 shows a cross-sectional view of the reactor. The CH_4 and N_2O, fed from different lines, both entered the reactor through the same inlet. The microwave plasma source directly excited these two gases, while SiH_4 entered the chamber away from the plasma source and was not directly excited. The peak maximum power, unless otherwise indicated, was 2300 W. The microwave source was pulsed on for 6 ms and then off for 16 ms.

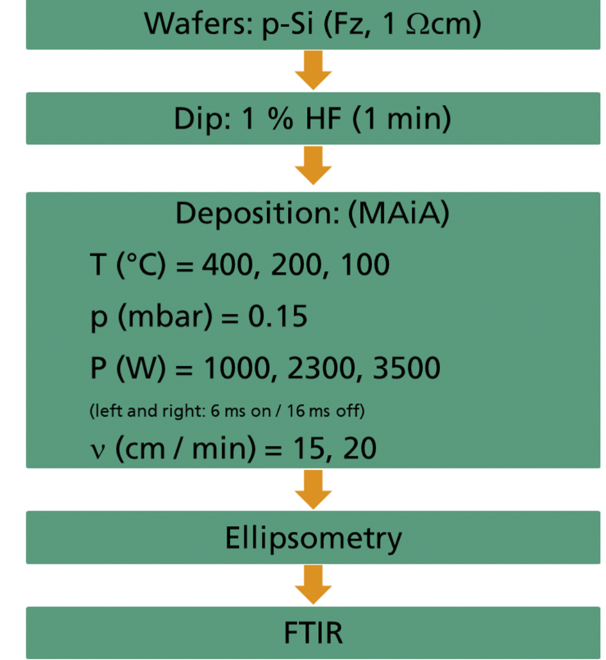

FIG. 1. Diagram of the experimental procedure showing the process flow and an overview of the deposition conditions. T stands for the deposition chamber temperature, p for the chamber pressure, P for the microwave power, and v for the carrier velocity.

© Author(s) 2020

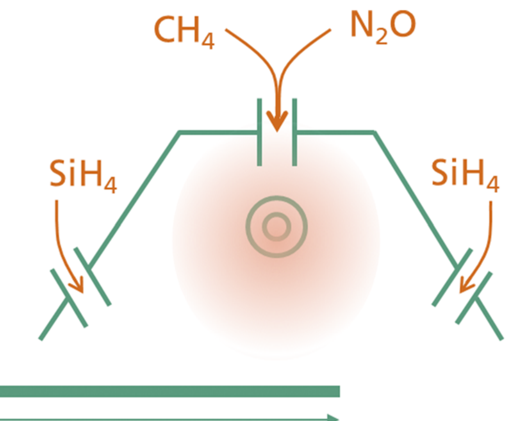

FIG. 2. Schematic cross-sectional view of the MAiA PECVD reactor showing gas inlets, plasma source, and the carrier direction (at the bottom of the sketch).

The deposition conditions for the experiments reported in this work are presented in Table I. To allow for better comparison between deposition conditions, the ratio of N_2O to SiH_4 was kept essentially constant at 18. Previous work (results not shown) indicated that a lower ratio (of 5) did not lead to a decrease in the refractive index of the deposited layers. In order to keep this ratio constant while increasing the ratio of CH_4 to N_2O, the percentage of SiH_4 was slightly decreased. The total gas flow was kept at either 1000 SCCM or 600 SCCM. The speed of the carrier was also kept roughly constant (at 15 cm/min or 20 cm/min). The thickness of the deposited layers ranged from 57 nm to 110 nm, as measured by ellipsometry. For each run under a given experimental condition, two samples were placed in the same spot on the carrier. For each experiment, the run order was randomized at a given deposition temperature.

D. Ellipsometry

Ellipsometry measurements were carried out using an M-2000 spectroscopic ellipsometer (J.A. Woollam) controlled with the CompleteEASE software (J.A. Woollam).[8] The optical parameters delta and psi were measured in the wavelength range of 193–1690 nm at three angles (65°, 70°, and 75° from normal). Using CompleteEASE, the following procedure was used to create a model to fit the measured data:[8]

(1) The parameters A, B, C, and thickness were fit for a Cauchy[9] layer on top of a Si_Jaw substrate.
(2) The Cauchy layer was parameterized with a Tauc–Lorenz (T–L)[10] layer.
(3) The T–L parameters of Amp1, Br1, Eo1, Eg1, and thickness were fit, first for the imaginary part of the spectrum and then for the imaginary and real parts.
(4) Using this layer, along with the T–L parameters, thickness, and roughness were fit and the parameters of refractive index (n, at 632.8 nm) and absorption coefficient (k, at 300 nm) were derived.

This model (see Fig. 3) was used for all of the deposited layers, as the same procedure was appropriate for the SiO_x layers as well as SiO_xC_y layers. For all samples, the root mean square error of the model, as calculated by the CompleteEASE program, was below 7.0, indicating a good fit. Unless otherwise stated, all ellipsometry measurements were performed on the same day as the depositions.

E. FTIR

FTIR spectra were collected in the range of 500–4000 cm^{-1} using a Vertex 80v FTIR spectrometer (Brucker Optik GmbH) controlled with the OPUS software (Brucker Optik GmbH).[11] An automatic sample wheel was used. All measurements consisted of the average of 75 scans. The spectral resolution was 8 cm^{-1}. The IR detector was cooled for roughly 30 min prior to the start of

TABLE I. N_2O to SiH_4 ratio; CH_4 to N_2O ratio; percentage of CH_4, N_2O, and SiH_4 in the process gas mixture; total process gas flow (SCCM); reactor chamber pressure (mbar); and carrier speed (cm/min) for SiO_x deposited without CH_4 in the process gas mixture and with three increasing levels of CH_4.

	N_2O/SiH_4	CH_4/N_2O	CH_4 (%)	N_2O (%)	SiH_4 (%)	Total gas (SCCM)	Pressure (mbar)	Carrier speed (cm/min)
SiO_x with no CH_4 addition	18.01	0.00	0	94.7	5.3	600.8	0.15	15[a]
	18.06	0.00	0	94.8	5.2	1000.5	0.15	20[b]
SiO_x with low CH_4 addition	18.06	0.33	24	72	4	600	0.15	15[a]
	18	0.33	24	72	4	1000	0.15	20[b]
SiO_x with high CH_4 addition	18	0.53	33.5	63	3.5	600	0.15	15[a]
SiO_x with highest CH_4 addition	18	0.80	43	54	3	600	0.15	15[a]

[a]At deposition temperatures of 100 °C and 200 °C.
[b]At a deposition temperature of 400 °C.

© Author(s) 2020

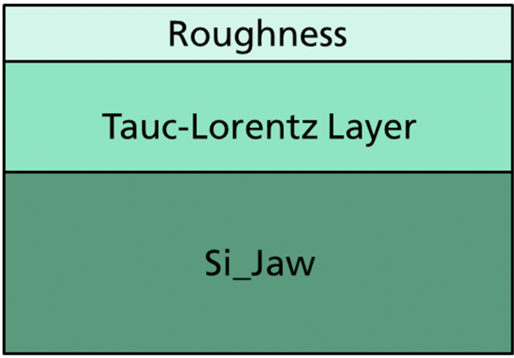

FIG. 3. Diagram of the model used to fit the ellipsometry data.

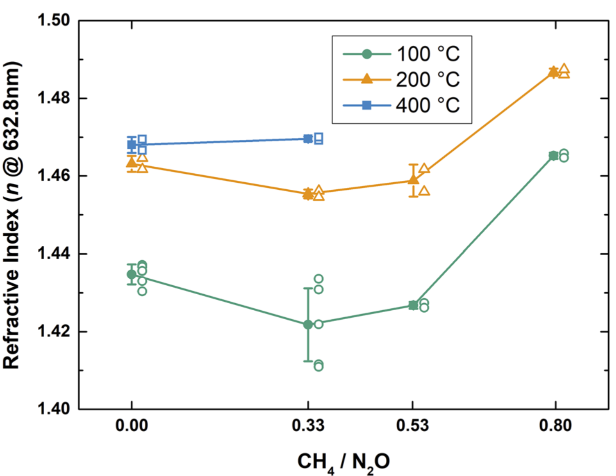

FIG. 4. Refractive index (n) vs ratio of CH_4 to N_2O for three deposition temperatures (100 °C, 200 °C, and 400 °C). The open symbols are individual measurements and the closed symbols are the mean for each condition. The error bars delineate one standard deviation. The solid lines are a guide for the eye. As a note, the ratio of N_2O to SiH_4 was kept approximately constant (at 18), which necessitated decreasing the percentage of SiH_4 from near 5% to near 3% as the CH_4/N_2O ratio increased. The total gas flow for the samples deposited at 400 °C was 1000 SCCM, for those deposited at 200 °C and 100 °C, the total gas flow was 600 SCCM.

the measurements using liquid nitrogen in order to improve the signal-to-noise ratio. Measurements were performed under vacuum to reduce interference with the IR signal due to ambient contaminants. After reaching vacuum, a background was taken. The measured spectra were subtracted from the background and that of a substrate consisting of the same material without a deposited layer to account for absorption due to the silicon base material. The spectra were then baseline corrected using the Automatic Baseline Correction function in the OPUS software. Due to noise below 550 cm^{-1} hindering an accurate baseline, some spectra were cut off manually below this point prior to the correction. The spectra were fit with a minimum number of Gaussian peaks using the Fityk software program.[12] The error, based on one standard deviation, was fully propagated when determining the ratio of the areas underneath the Gaussian bands.

F. OES

OES spectra were collected using an Emicon SA (Plasus) spectrometer. The spectral resolution was 1.5 nm. Spectra, from 200 nm to 900 nm, were collected once the plasma reached a steady state.

III. RESULTS

A. Ellipsometry

1. Temperature and gas ratio variations

The refractive indices of the deposited layers at a wavelength of 632.8 nm, determined by fitting a spectroscopic ellipsometry model to our measured spectra, are presented in Fig. 4 as a function of the process gas mixture (represented as the ratio of CH_4 to N_2O) at three deposition temperatures (400 °C, 200 °C, and 100 °C). Both the individual measurements and the mean (with the associated standard deviation) are shown. As a note, the k values (at 300 nm) were below the very small value of 0.0005 for all samples indicating little light absorption.

The temperature had the largest effect on the refractive index. At lower temperatures, regardless of the other deposition conditions, the deposited layers had lower refractive indices (see Fig. 4). The difference in the n values of the layers deposited at a temperature of 400 °C (blue squares) and 200 °C (orange triangles) was not as drastic as the difference between those deposited at 100 °C (green circles). For example, the average refractive indices of the SiO_x deposited at 400 °C and 200 °C without CH_4 in the process gas mixture were both roughly 1.47, whereas at 100 °C the average refractive index of the deposited layers was just below 1.44. In addition to the deposition temperature, the CH_4 content of the process gas mixture also affected the refractive index.

At a deposition temperature of 400 °C, adding CH_4 slightly increased the average n value (see Fig. 4). At deposition temperatures of 200 °C and 100 °C, as the percentage of CH_4 in the process gas mixture initially increased to a CH_4 to N_2O ratio of 0.33, the refractive indices of the layers decreased slightly. We would caution that this decrease was slight, and the magnitude of the decrease was inconsistent across repetitions of the deposition conditions, as seen in the range of measured values for our prepared samples. While this prevents us from making a strong claim to the decrease in the refractive indices, one standard deviation in the measurements of those deposited at 100 °C and 200 °C and CH_4 to N_2O ratios of 0.00 and 0.33 do not overlap. This indicates that there is support for the claim that the refractive index did decrease initially with the introduction of CH_4.

As the CH_4 to N_2O ratio increased to 0.53, the refractive index of the deposited layers at 200 °C rose slightly and became consistent considering a standard deviation with the SiO_x layers. While at 100 °C, the refractive index remained below that of SiO_x. At deposition temperatures of 200 °C and 100 °C, the refractive indices of the deposited layers at a CH_4 to N_2O ratio of 0.80 increased significantly above that of SiO_x.

As a note, the total gas flow for the samples deposited at 400 °C was 1000 SCCM and 600 SCCM for those deposited at 200 °C and

© Author(s) 2020

100 °C. While not shown here, the difference in the refractive indices between the layers deposited at 200 °C from total gas flows of 1000 SCCM and from 600 SCCM for both SiO_x layers deposited without CH_4 in the process gas mixture and layers with a CH_4 to N_2O ratio of 0.33 was very small. We therefore concluded in this range, the total gas flow did not have a large effect on the refractive index. As it was important to narrow the variable space, considering the many possible process parameters, the effect of the total gas flow was not characterized in this study.

2. Power variations

The refractive index of the SiO_x layers deposited at 100 °C and three increasing maximum microwave powers (1000 W, 2300 W, and 3500 W) with no CH_4 in the process gas mixture and at a ratio of CH_4 to N_2O of 0.33 is shown in Fig. 5. At all three maximum power values, the refractive index of the layers decreased upon adding CH_4 to the process gas. However, the magnitude of change in n increased along with increasing maximum power.

3. Stability

The layers deposited at 100 °C, which had the lowest n values and showed the largest effect of adding CH_4 to the process gas mixture, were not stable over time. After two months of storage in the dark in a plastic wafer box, the refractive indices for all the layers rose (see Table II). Except for the highest level of CH_4 in the process gas mixture, the other three conditions approached n = 1.46–1.47, which is the refractive index of SiO_2. For the highest level of CH_4, n rose relatively the least with time, though it rose above the refractive index of SiO_2. This pattern was the same for the samples deposited at 200 °C and 600 SCCM total gas flow (results not shown).

B. FTIR

1. Bonding

Normalized FTIR spectra, from 500 cm^{-1} to 4000 cm^{-1} with a resolution of 8 cm^{-1}, of the layers deposited at 400 °C (total gas flow = 1000 SCCM) and at 100 °C and 200 °C (total gas flow = 600 SCCM) with increasing CH_4 flow in the process gas mixture are shown in Fig. 6. The main feature in all the spectra was the band between 850 cm^{-1} and 1250 cm^{-1}, representing the various modes of the Si–O–Si bond.[3] As a note, none of the spectra showed any clear characteristic silicon oxycarbide (SiO_xC_y) features, most notably the Si–CH_3 band near 1260 cm^{-1}.[13,14]

A more detailed investigation was carried out in the types of bonds and bonding configuration found in the layers by fitting the unnormalized spectra with a minimum number of Gaussian peaks in the range of roughly 700–1500 cm^{-1} (see Table III). This deconvolution yielded either three or four peaks. We assigned the peak near 800 cm^{-1} to the Si–O–Si bending mode, the main peak near 1050 cm^{-1} to the Si–O–Si stretching mode, and the shoulder near 1160 cm^{-1} to the Si–O–Si stretching in a more open structure or near

TABLE II. CH_4 to N_2O ratio, single measurements of n (at 632.8 nm) for the same layer the day of the deposition (t = 0) and after two months and the change in n.

	CH_4/N_2O	n (at 632.8 nm) t = 0	n (at 632.8 nm) t = 2 months	Δn
SiO_x with no CH_4 addition	0.00	1.436	1.469	0.033
SiO_x with low CH_4 addition	0.33	1.412	1.461	0.049
SiO_x with high CH_4 addition	0.53	1.427	1.462	0.035
SiO_x with highest CH_4 addition	0.80	1.466	1.481	0.015

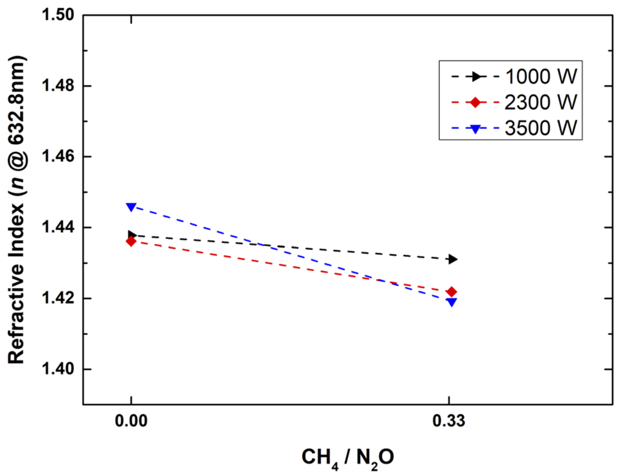

FIG. 5. Average refractive index vs CH_4/N_2O for the layers deposited at three different maximum powers. The deposition temperature was 100 °C. The dashed lines are a guide to the eye.

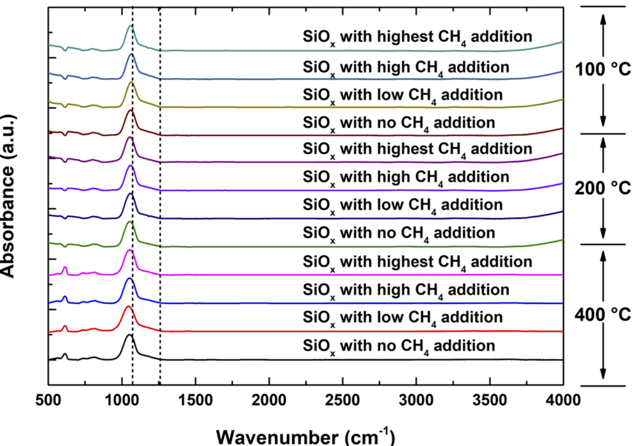

FIG. 6. Normalized FTIR absorbance spectra from 500 cm^{-1} to 4000 cm^{-1} for the layers deposited with increasing CH_4 flows at a deposition temperature of 400 °C (total gas flow = 1000 SCCM) and at deposition temperatures of 200 °C and 100 °C (total gas flow = 600 SCCM). The dashed, vertical lines indicate the center of the main Si–O–Si stretching peak at 1050 cm^{-1} and the characteristic Si–CH_3 band at 1260 cm^{-1}.

© Author(s) 2020

TABLE III. Ratio of CH_4 to N_2O and average fitted Gaussian peak location (cm^{-1}) for three deposition conditions and the corresponding levels of CH_4 in the process gas mixture.

Deposition conditions		CH_4/N_2O	Peak position at ~800 cm^{-1}	Peak position at ~960 cm^{-1}	Peak position at ~1050 cm^{-1}	Peak position at ~1150 cm^{-1}
400 °C 1000 SCCM	SiO_x with no CH_4 addition	0.00	797	...	1051	1168
	SiO_x with low CH_4 addition	0.33	786	...	1052	1166
200 °C 600 SCCM	SiO_x with no CH_4 addition	0.00	811	...	1052	1164
	SiO_x with low CH_4 addition	0.33	810	...	1056	1162
	SiO_x with high CH_4 addition	0.53	808	...	1057	1160
	SiO_x with highest CH_4 addition	0.80	803	966	1053	1151
100 °C 600 SCCM	SiO_x with no CH_4 addition	0.00	809	...	1056	1160
	SiO_x with low CH_4 addition	0.33	807	...	1062	1154
	SiO_x with high CH_4 addition	0.53	807	...	1061	1152
	SiO_x with highest CH_4 addition	0.80	801	957	1056	1146

a void.[5,13] These three peaks were present in all samples and correspond to the SiO_x layer. As a note, the lack of Si–N[15] or SiC_yN_z[16] features (in both cases, a strong absorption band centered near 850 cm^{-1}) indicated that neither SiO_xN_z nor SiC_yN_z was deposited.

Assigning the band near 950 cm^{-1} was more challenging, as there are different explanations in the literature: absorption due to dangling bonds in the Si–O–Si lattice[5] or due to Si–CH_3.[14] In our samples (see Table III), the band near 960 cm^{-1} in the FTIR spectra of the layers deposited from the highest CH_4 content (CH_4/N_2O = 0.80, CH_4 content = 43% of the process gas mixture) was likely due to Si–CH_3 bonding.[14] The appearance of this peak corresponded with the blue shift of the shoulder near 1160 cm^{-1} to near 1150 cm^{-1}. (At both deposition temperatures of 100 °C and 200 °C, this shift was greater than the 8 cm^{-1} resolution of our measurements.) In the literature, this shoulder of the broad Si–O–C peak at 1100 cm^{-1} represents a Si–O–C cage-link structure corresponding to a porous SiO_xC_y layer.[14] Taken together, these two peaks support that the SiO_xC_y layers were formed at higher CH_4 flows.

2. Porosity

FTIR was used to classify the porosity of the layers. As mentioned previously, the shoulder near 1160 cm^{-1} arises from Si–O–Si stretching in a more open structure or near a void.[4] In the literature, the ratio of the areas underneath this shoulder and the main Si–O–Si stretching peak near 1050 cm^{-1} has been shown to correlate with the porosity of the SiO_x layers.[4] The averages of this ratio for our samples deposited at 400 °C, 200 °C, and 100 °C as a function of the CH_4 to N_2O ratio in the process gas mixture are shown in Fig. 7.

At all gas ratios of CH_4 to N_2O, the area ratio was higher for lower deposition temperatures (see Fig. 7). For a deposition temperature of 100 °C, this ratio quickly rose as the ratio of CH_4 to N_2O increased from 0.00 to 0.33. As the gas ratio increased further, the area ratio then decreased. At a deposition temperature of 200 °C, the area ratio increased steadily with increasing gas ratio. For a deposition temperature of 400 °C, the trend was reversed compared to the other experimental conditions, with the area ratio decreasing as the gas ratio increased from 0.00 to 0.33. No experiments for higher gas ratios at 400 °C were performed.

C. OES

OES spectra were collected at a total gas flow of 600 SCCM and a deposition temperature of 100 °C for CH_4 to N_2O ratios of 0.00 and 0.33 to gain insight into the plasma conditions (see Fig. 8). The spectrum of the plasma without CH_4 was subtracted from the spectrum when CH_4 was in the process gas mixture to see the change in emission band intensities. As seen in Fig. 8, with the addition of CH_4 there was an increase in the peaks near 486 nm and 656 nm, representing, respectively, the beta (Hb) and alpha (Ha) modes of hydrogen (2nd and 1st transitions of the Balmer series).[17]

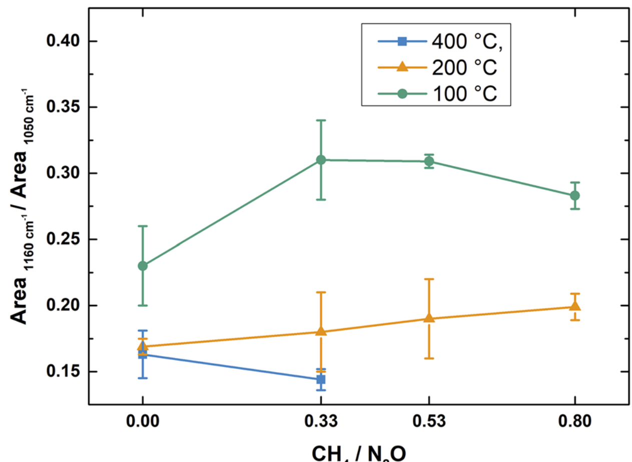

FIG. 7. Ratio of the area under the shoulder near 1160 cm^{-1} to the area under the main peak near 1050 cm^{-1} vs the ratio of CH_4 to N_2O in the process gas mixture for the layers deposited at three deposition temperatures. This ratio corresponds to the porosity in the SiO_x layers. The error bars represent the propagated error based on one standard deviation.

© Author(s) 2020

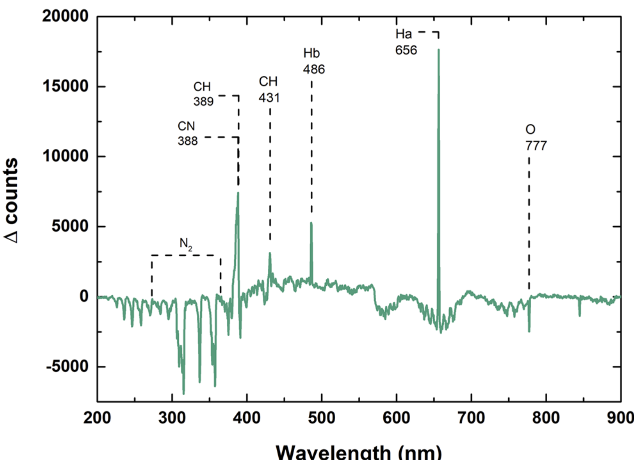

FIG. 8. Change in OES emission spectra in the range of 200–900 nm upon the addition of CH_4 (from CH_4/N_2O = 0.00–0.33) at 100 °C with a total gas flow of 600 SCCM while keeping the OES tool settings constant.

Additionally, two peaks, at 389 nm and 431 nm, representing CH species appeared.[17] One should note that the peak for CN is found at 388 nm.[17] The precision of our OES setup (1.5 nm) did not allow us to resolve the peaks for CH and CN. Furthermore, there may be other CH_n-containing species (such as CH_3 or C_2H_2) in the plasma, but only CH and C_2 produce detectable fluorescence.[18] In our case, the most intense emission bands of C_2 (near 512 nm and 516 nm)[17] were indistinguishable from the background noise (see Fig. 8). Finally, from Fig. 8, it is clear that the peaks between roughly 300 nm and 370 nm, representing various N_2 emissions decreased with the addition of CH_4 and the corresponding decrease in N_2O.[17] Along with this decrease, the characteristic O peak, near 777 nm, also decreased.[19]

IV. DISCUSSION

A. Optical properties

For the refractive index of the deposited SiO_x layers, we propose two regimes based on the CH_4 content in the process gas mixture and the deposition temperature. The main characteristic of the first regime was that adding CH_4 to the process gas mixture decreased the refractive index. For a deposition temperature of 100 °C, the first regime consisted of a ratio of CH_4 to N_2O up to 0.53 (or 33.5% CH_4 in the process gas mixture). At this ratio, the average refractive index of the deposited layers decreased compared to the SiO_x layers deposited without CH_4 (see Fig. 4). For a deposition temperature of 200 °C, the first regime consisted of a ratio of CH_4 to N_2O up to 0.33.

This behavior can be explained by an increase in porosity in the layers. In this regime, as measured by FTIR, the layer porosity was the greatest for a deposition temperature of 100 °C followed by a deposition temperature of 200 °C (see Fig. 7). This trend corresponded to the layers deposited at lower temperatures having lower refractive indices (see Fig. 4). Since n_{air} = 1.0, increasing the layer porosity will increase the percentage of voids in the layer and will decrease the effective refractive index of the layers.

The temporal stability of the layers deposited at 100 °C also indicated that the porosity increased initially with the addition of CH_4 to the process gas mixture (see Table II). More porous layers, with more reaction sites, would oxidize at a faster rate than less porous layers. After two months of storage under ambient conditions, the layers grown with a gas ratio of 0.33 had the largest increase in *n*. As a note, the refractive indices of all the layers (except those with the highest CH_4 content in the process gas mixture) reached roughly 1.47 after two months. This is most likely due to the fact that an uninterrupted SiO_x lattice would be more energetically favorable than an incomplete lattice. Therefore over time, the layers under ambient conditions would oxidize via reactions with moisture or O_2 (g) resulting in rearrangement in the lattice. This possible explanation is supported by the small change in the measured thickness of the layers (a decrease of <1 nm for all layers) after two months indicating no oxide growth on the layers but rather a change in the layers themselves.

Further support for the connection between the porosity and the refractive index is that at a deposition of 400 °C, the average *n* value of the deposited layers increased along with a *decrease* in the layer porosity (see Figs. 4 and 7). This indicated that under our deposition conditions, the first regime only existed at deposition temperatures of 100 °C and 200 °C.

In the second regime, the increasing CH_4 content increased the refractive index compared to SiOx deposited without CH_4 in the process gas mixture. In our experiments, this regime depended on the deposition temperature. For 100 °C, the regime consisted of a CH_4 to N_2O ratio of 0.80 (or 43% CH_4 in the process gas mixture). For 200 °C, the regime consisted of CH_4 to N_2O ratios of 0.53 and 0.80 (or 33.5% CH_4 and 43% CH_4 in the process gas mixture, respectively). Under these conditions, the average refractive index of the deposited layers rose along with increasing CH_4 flow (see Fig. 4). The porosity, from the FTIR measurements, however, stayed roughly constant compared to the samples deposited with lower amounts of CH_4 in the process gas mixture (see Fig. 7).

A possible explanation of the behavior in the second regime involves the formation of silicon carbide bonds in the layers. The refractive index of Si–C is near 2.0. An increase in the Si–C bonding concentration would therefore increase a layer's refractive index, potentially countering any effect of increase in the porosity. For the highest CH_4 concentrations in the process gas mixture, the fitted FTIR spectra indicated the formation of Si–C and Si–O–C features in the deposited layers (see Table III). For the second highest CH_4 concentration in the process gas mixture, the rise in the refractive index compared to the lowest CH_4 concentration was small for both deposition temperatures (see Fig. 4). In the FTIR spectra, we did not observe the characteristic Si–CH_3 band near 950 cm^{-1} (see Table III). We also only measured a very slight blue shift (2 cm^{-1}) in the shoulder near 1150 cm^{-1}, though the spectral resolution of our measurements (8 cm^{-1}) prevents us from making any strong claim to that effect. It is possible that the process of fitting the FTIR spectra was not sensitive enough to detect a very small increase in Si–C or Si–O–C bonding. It is also possible that the first regime included these CH_4 to N_2O ratios as well and that more experimental measurements would show that the rise in *n* values only took place at the highest CH_4 content in the process gas mixtures. A more

© Author(s) 2020

accurate characterization technique, such as XPS, could potentially give more insight into the elemental composition of the layers. In order to better understand the complex interactions between the deposition temperature and process gas mixture, we formulated a possible growth and reaction pathway.

B. Plasma-enhanced oxide growth model

To better understand the growth mechanism and the surface processes of the two experimental regimes, we developed a model based on our results. We should note that the plasma growth is characterized by a multitude of reactions and reaction pathways. This is due to the high energies involved, which facilitates the formation of many active species. The surface processes involved in PECVD are also complex, with adsorption, desorption, and film growth all occurring in tandem and affected by both local growth and plasma conditions.[20] Here, we propose a possible reaction pathway, focused on surface chemistry, to help better conceptualize our results. This pathway, if an accurate representation of reality, would surely be the only one possible reaction route competing among many. In fact this competition between growth pathways, as discussed later, may help explain the experimental results.

Both surface conditions and plasma conditions were likely to play a role in the growth and correlated characteristics of our layers. The temperature dependence of the layer properties (refractive index and porosity) indicated the importance of surface processes. While influencing the surface chemistry and layer growth, the deposition temperature would not play a critical role in the plasma composition with all other processing conditions held constant. Furthermore, if surface processes were the controlling factors in the layer growth, then the amount of activated species reaching the surface would play a minor role. This was not, however, the case. In general, increasing the maximum power increases the flux of active species reaching the surface of the samples. We found that there was a larger change in n upon increasing the CH_4 flow from 0.00% to 0.24% at higher peak microwave powers (see Fig. 5). This maximum power and hence the flux of active species reaching the surface had an effect on the layer properties, which indicated that the plasma conditions played a role in the layer properties. In our chemical model, we therefore considered both surface and plasma processes (see Fig. 9). Figure 9 presents a generalized reaction pathway. The reactive species shown represent many possible reactants and the reactions presented certainly neglect possible intermediate species and steps.

We first considered the silicon surface. Our initial assumption was the surface was Si–H terminated, as would be the case after the HF dip we performed directly before deposition. Next, during exposure to the plasma, we proposed that the hydrogenated surface would be dominated by Si–O–H bond formation (see the surface reaction by the O-species in Fig. 9). This assumption was based on Aydil and Han's work characterizing the SiO_2 growth from SiH_4 and O_2 plasmas.[20] They reported that for a high ratio of SiH_4 to O_2, the flux of oxygen reaching the surface would be greater than the SiH_4 fragments. This would cause the O atoms to oxidize any Si–H bonds on the surface. For our experiments, the ratio (at 18) of N_2O (which in plasma forms O-species) to SiH_4 was very high, which supported this assumption.

Next, we looked at the contribution of methane in the plasma. Based on the literature of CH_4 plasmas, we assumed that active CH_x and larger CH-containing species (such as C_2H_x) were formed.[3,18] From our OES data, we could detect CH (the only OES-active CH-species) (see Fig. 8). From the OES spectrum, it is clear that there was also a large increase in H-emissions in the plasma. An increase in H would be important for H-facilitated reaction pathways.

Combining the surface model consisting of the formation of Si–O–H bonding and the likely presence of CH_3, other CH-containing species, and active hydrogen, we proposed a growth mechanism accounting for our experimental results. The first step would be the reaction, possibly with surface dangling bonds or via H-abstraction, between active CH-species and H with surface Si–O–H bonds.[21] This would result in various O- and C-containing complexes based on the exact reactants. Figure 9 shows the formation of one such intermediate, resulting from the reaction between a CH-species and the Si–O–H surface to form a possible Si(OH)(CH) surface complex.

From here, the surface would be similar to those found in the careful study by Yanguas-Gil *et al.*[22] In that work, $SiO_xC_y:H_z$ films were formed from oxygen–tetramethylsilane mixtures. Due to

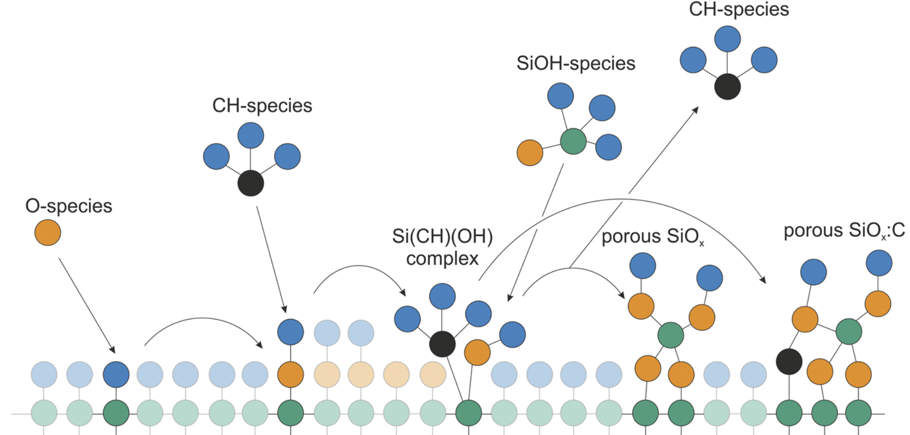

FIG. 9. A chemical model of the proposed growth pathway. The green circles represent Si atoms, the orange O, the blue H, and the black C. As a note, the O-, CH-, and SiOH-species represent many possible reactants and combinations of reactants. All possible reactions (including many possible hydrogen-facilitated reactions) are not shown. Whether carbon is incorporated into the layer during the final step is most likely determined by the flux of SiOH-species (and other SiO_x precursors) that reaches the surface. Additionally, the formation of SiO_x and SiO_x:C at the substrate surface from, for example, SiH_x, O, and CH_x species, is likely.

© Author(s) 2020

different starting materials, the reaction pathway to form silicon–oxygen–carbonyl surface complexes in their study would most likely be different than that under our reaction conditions. However, we assume that once formed, a condensation reaction involving the silicon–oxygen–carbon surface complexes and oxidized Si fragments (in our case, most likely oxidized SiH_x species[23]) to form the SiO_x layers would be similar.[22] A reaction between a plasma SiOH-species, of which there are many possibilities, and the SiCOH surface complex, of which there are also many possibilities, is shown in Fig. 9.

In terms of carbon incorporation into the films, Yanguas-Gil *et al.* proposed that the most important factor was the oxygen concentration reaching the surface. Low O concentrations led to the layers with more Si–C bonding (as measured with XPS). Higher O concentrations lead to the layers with almost no C incorporation.[22] In our proposed growth pathway (see Fig. 9) at high O concentrations, this final growth step involves desorption of any CH-species.[24] However, in another possible final growth step under low O concentrations, the CH-species could be incorporated into the growing layer.

Whether eventually desorbed or incorporated, the CH-species would alter the steric and electrical environment of the surface compared to the competing growth pathway of normal SiO_x formation.[13] Figure 9 shows two final growth steps in the proposed reaction pathway. The growth step under high-oxygen conditions (resulting in porous SiO_x) would be somewhat analogous to that described in the work by Barranco *et al.*, in which the authors used a sacrificial organic layer that initially formed a highly oxygenated surface SiOCH complex.[7] This surface complex affected the porosity of the layer by disrupting the growth and served as a nucleation site for the SiO_x growth, while simultaneously being removed by SiO_x-precursor species in the plasma. In our pathway under low-oxygen conditions, there is too low a flux of oxidized SiO_x precursors to desorb all the CH bonded in surface complexes. Therefore, as the layer grows—a process involving the continuous adsorption, desorption, and movement of species—there is a higher probability that some C is incorporated into the film.

Our growth pathway may explain the dependence on the CH_4 to N_2O ratio in the process gas mixture. An important note is that since the total gas flow was kept constant, increasing CH_4 in the process gas mixture decreased the amount of N_2O. Since N_2O was the source of O-species in the plasma, adding CH_4 decreased the O content in the plasma. This is clear in Fig. 8, as the O peak at 777 nm decreased with the addition of CH_4 to the process gas mixture. Our two regimes can then be thought of as low CH_4/high O and high CH_4/low O. In the first regime, CH-species contribute to intermediate complexes on the surface. However, the high O flux reaching the surface would cause CH-species to desorb. While there would be little to no C-incorporation into the layers, the altered growth mechanism would increase the inhomogeneity and porosity of the films. In the second regime, there would be a greater CH-species flux and a lower O-species flux reaching the surface. This would increase the chance that a CH-species would not be desorbed as the SiO_x layer grew. Consequently, Si–C bonding in the layers would increase.

This model may also explain the temperature dependence of the effect of CH_4 lowering the refractive index of our layers in the first regime. There are two possible explanations. The first assumes that dangling bonds are the reaction sites for the carbon-mediated growth mechanism. This assumption is based on the growth of amorphous carbon layers[21] and may not be applicable to SiO_x films. At lower deposition temperatures there is less homogeneous growth.[25] This is the reason that the SiO_x layers without CH_4 in the process gas mixture grown at lower temperatures had lower n values than those grown at higher temperatures (see Fig. 4). At the highest deposition temperature (400 °C) more homogeneous growth may have decreased the available surface dangling bonds. If dangling bonds are the reaction sites for the proposed carbon-mediated growth pathway, then a higher temperature would favor other growth mechanisms (such as those that produce less porous SiO_x). This could explain why adding CH_4 to the process gas mixture did not have a large effect on the layers deposited at 400 °C (see Fig. 4). For lower deposition temperatures, less homogeneous growth would mean that there were more surface dangling bonds and therefore more reaction sites for CH-species. Since other growth pathways (potentially leading to more homogeneous, less porous layers) would always compete with CH-regulated growth pathways (potentially leading to less homogeneous layers), more reactive sites could increase the chance of CH-species reacting with the surface. Therefore, at lower deposition temperatures, the effect of adding CH_4 to the process gas mixture would be greater. If this mechanism is correct, then adding an inert gas, such as He or Ar, to increase the dangling bond concentration via surface damage (ion bombardment of the substrate or previously grown layer) could increase the layer porosity.

Another possible explanation lies with the interplay between adsorption and desorption, both of which can be affected by the substrate temperature. This scenario involves a greater temperature dependence for desorption than adsorption of CH-species. At high temperatures, this would cause rapid desorption of any adsorbed species without the aid of SiO_x precursors. A result would be non-carbon-mediated, less porous growth. However, at lower temperatures, adsorption would be less hindered by the lower temperature than desorption. Therefore, a slow rate of desorption would increase the probability that a SiO_x precursor could react with or at the site of a surface CH-containing complex. This process could then disrupt the SiO_x growth (or possibly lead to C-incorporation) via a reaction pathway potentially similar to that in Fig. 9. If the difference in adsorption and desorption rates is a dominant feature of this growth pathway, then increasing this difference via modifying the substrate chemistry or by depositing layers at lower temperatures could increase the layer porosity.

V. CONCLUSION

This work characterized the effect on the refractive index of adding CH_4 to the standard process gas mixture for PECVD SiO_x growth in an industrial scale microwave reactor. We proposed the existence of two regimes based on the CH_4 flow and deposition temperature. In the first, adding CH_4 decreased the refractive index of the deposited layers due to an increase in the porosity of the layer. In the second regime, increasing CH_4 flows led to layers with increasing n values compared to the SiO_x layers grown without CH_4 in the process gas mixture, without a marked change in the porosity. FTIR spectra indicated an increase in Si–C

© Author(s) 2020

and Si–O–C bonding features in the layers deposited in the second regime, which would account for the increase in the *n* values. Deposition temperatures also played a role, with lower deposition temperatures giving the layers with lower refractive indices. At lower deposition temperatures, the effect of CH_4 on changing the refractive index was also greater. Power variation experiments indicated that plasma conditions, in addition to surface processes, played a role in these observed effects. OES measurements gave insight into the effect on the plasma of adding CH_4 to the process gas mixture. Furthermore, we proposed a possible growth pathway accounting for plasma and surface conditions to help explain our results.

From an application point of view, the magnitude of the decrease in *n* was not great and the layers were not stable over time in air at room temperature (potentially with further oxidation or densification leading to the refractive index increasing and approaching that of standard SiO_x). These results show that our deposited layers would not find application in industrial processes.

Further work could determine the effects of deposition pressure, carrier speed, and maximum power and on/off timing of the plasma source on lowering the refractive index of the deposited layers and on increasing their stability. While the range of gas flows was limited by our mass flow controller (MFC), future experiments could look at higher N_2O to SiH_4 ratios, which could allow for higher CH_4 to N_2O ratios, thereby extending the range of the first regime. In that case, if our proposed growth pathway is accurate, higher O-species fluxes reaching the silicon surface could prevent the formation of Si–C and Si–O–C bonding while allowing the CH-species to further disrupt the SiO_x bonding network. Adding argon or He to the process gas mixture could also potentially cause further damage to the SiO_x lattice, thereby increasing the porosity and/or potentially creating more reactive sites for the CH-mediated, porous SiO_x growth. The stability of the layers also needs to be addressed. By controlling the morphology of the voids introduced into the layers, more cross-linking could increase the layer stability to further oxidation and the scratch resistance.[6] Finally, the increase in hydrogen species in the plasma upon adding CH_4 could be beneficial when depositing SiO_x on top of the SiN_x or AlO_x passivating layers in a stacked passivating/anti-reflection design such as those found on solar cells. For many applications of the layers, further understanding of the growth and structural properties of PECVD-grown SiO_x will be critical.

ACKNOWLEDGMENTS

B.T. would like to thank the German–American Fulbright Commission for support in the form of a study/research grant. We thank the German Federal Ministry for Economic Affairs and Energy (BMWi) for its financial support under Contract No. 0324171B.

REFERENCES

[1] J.-Q. Xi, M. F. Schubert, J. K. Kim, E. F. Schubert, M. Chen, S.-Y. Lin, W. Liu, and J. A. Smart, Nat. Photonics **1**, 176 (2007).
[2] H. Nagel, A. G. Aberle, and R. Hezel, Prog. Photovoltaics: Res. Appl. **7**, 245 (1999).
[3] E. Gil, J. B. Park, J. S. Oh, and G. Y. Yeom, Thin Solid Films **518**, 6403 (2010).
[4] H. Nagel, A. Metz, and R. Hezel, Sol. Energy Mater. Sol. Cells **65**, 71 (2001).
[5] J. S. Chou and S. C. Lee, J. Appl. Phys. **77**, 1805 (1995).
[6] H. Kakiuchi, H. Ohmi, Y. Yamaguchi, K. Nakamura, and K. Yasutake, Thin Solid Films **519**, 235 (2010).
[7] A. Barranco, J. Cotrino, F. Yubero, J. P. Espinós, L. Contreras, and A. R. González-Elipe, Chem. Vap. Deposition **10**, 17 (2004).
[8] J.A. Woollam Co., Inc., CompleteEASE Data Analysis Manual, 2011.
[9] F. A. Jenkins and H. E. White, *Fundamentals of Optics*, 4th ed. (McGraw-Hill Book Company, New York, NY, 1981).
[10] G. E. Jellison and F. A. Modine, Appl. Phys. Lett. **69**, 371 (1996).
[11] Bruker Optik GmbH, OPUS Reference Manual, 2004.
[12] M. Wojdyr, J. Appl. Crystallogr. **43**, 1126 (2010).
[13] V. Purohit, E. Mielczarski, J. A. Mielczarski, and L. Akesso, Mater. Chem. Phys. **141**, 602 (2013).
[14] R. Navamathavan, K. S. Oh, S. Y. Chang, S. H. Kim, Y. J. Jang, A. S. Jung, H. J. Lee, K. M. Lee, and C. K. Choi, Jpn. J. Appl. Phys., Part 1 **45**, 8435 (2006).
[15] F. Demichelis, F. Giorgis, and C. F. Pirri, Philos. Mag. B **74**, 155 (1996).
[16] C. Huber, B. Stein, and H. Kalt, Thin Solid Films **634**, 66 (2017).
[17] T. Vandevelde, M. Nesladek, C. Quaeyhaegens, and L. Stals, Thin Solid Films **290-291**, 143 (1996).
[18] P. B. Davies and P. M. Martineau, Adv. Mater. **4**, 729 (1992).
[19] M. Hur, J. O. Lee, J. Y. Lee, W. S. Kang, and Y.-H. Song, Plasma Sources Sci. Technol. **25**, 015008 (2016).
[20] S. M. Han and E. S. Aydil, Thin Solid Films **290-291**, 427 (1996).
[21] A. von Keudell, M. Meier, and C. Hopf, Diamond Relat. Mater. **11**, 969 (2002).
[22] Á. Yanguas-Gil, Á. Barranco, J. Cotrino, P. Gröning, and A. R. González-Elipe, Chem. Vap. Deposition **12**, 728 (2006).
[23] M. Riera, J. A. Rodríguez, J. Barreto, and C. Domínguez, Thin Solid Films **515**, 3380 (2007).
[24] K. Bera, B. Farouk, and P. Vitello, J. Phys. D: Appl. Phys. **34**, 1479 (2001).
[25] W. A. Seward and E. J. Jumper, J. Thermophys. Heat Transfer **5**, 284 (1991).

© Author(s) 2020